Limited microglial metabolic improvement with time-restricted feeding in diet-induced obesity

Han Jiao[1,2,3,4+], Jarne Jermei[1,2,3,4+], Xian Liang[5+], Felipe Correa-da-Silva[1,2,3,4], Milan Dorscheidt[1,2,3,4], Valentina Sophia Rumanova[1,2,3,4], Delaram Poormoghadam[1,2,3,4], Ewout Foppen[1,2,3,4], Nikita Korpel[1,2,3,4], Dirk Jan Stenvers[1,2,3,4], Alberto Pereira Arias[1,2,3], Tiemin Liu[6], Zhi Zhang[6], Andries Kalsbeek[1,2,3,4], Chun-Xia Yi[1,2,3,4*]

1. Department of Endocrinology and Metabolism, Amsterdam University Medical Centers, location AMC, University of Amsterdam, Amsterdam, The Netherlands.
2. Amsterdam Gastroenterology Endocrinology and Metabolism, Amsterdam, The Netherlands.
3. Department of Clinical Chemistry, Laboratory of Endocrinology, Amsterdam University Medical Centers, location AMC, Amsterdam, The Netherlands.
4. Netherlands Institute for Neuroscience, Amsterdam, The Netherlands.
5. Human Phenome Institute, Fudan University, Shanghai, China
6. State Key Laboratory of Genetic Engineering, School of Life Sciences, Fudan University, Shanghai 200438, P.R. China

+ These authors contributed equally to this work.

***Correspondence:**
Chun-Xia Yi
Department of Endocrinology and Metabolism
Amsterdam University Medical Centers, Location AMC
Meibergdreef 9, 1105 AZ Amsterdam
T: +31 20 5664807 | E: c.yi@amsterdamumc.nl

Abstract

Time-restricted eating has shown promise for improving metabolic health in obese humans. In this study, we investigated how time-restricted feeding (TRF) at different times of the day affects the microglial brain immune function using Wistar rats. We found that in high-fat diet (HFD)-induced obesity, TRF during the active phase of rats is effective in reducing fat mass, enhancing the rhythmicity of the microglial transcriptome, and preventing an increase in microglial cell number. These effects are not seen with TRF during the resting phase. However, the HFD-induced activation of microglial metabolic pathways was not reversed by TRF in either the active or resting phase, indicating that the reprogrammed microglial metabolism in obesity is a persistent cellular functional change that might form a metabolic memory and play a role in body weight regain upon discontinuation of restricted eating.

Main

The growing global obesity crisis and its associated complications poses major health concerns [1-3]. One of the causes of obesity in our modern society is associated with prolonged eating times and shorter fasting periods during the day-night cycle [4]. Time-restricted eating (TRE), by limiting eating time window and increasing the intermittent fasting period, has emerged as a novel strategy for preventive healthcare and metabolic disease management [5-12]. Both human and animal studies have demonstrated that alignment of the time restricted eating (or feeding in animal study) periods with the body's natural circadian rhythms is a crucial prerequisite for its beneficial effects [5, 8, 11, 13-17].

The immune activity in peripheral myeloid cells and brain microglia plays an important role during obesity development [18-24]. The immune processes in these immune cells tightly follow a circadian rhythmicity [25, 26], and the intrinsic core clock genes regulate key immune transcription factors that drive rhythmic expression of cytokines and function of immune receptors [26-31]. In addition, circadian proteins regulate inflammatory responses and immune cell trafficking [28, 29, 31-34]. Previous studies have shown that the rhythmicity in clock genes and immunometabolic pathways are disturbed when animals are subjected to an obesogenic high-fat diet (HFD) [35], possibly due to the fact that when fed a HFD their eating time is restrained anymore to the active (dark) period [36], but also extends into the resting (light) period when they usually sleep [5, 37]. The current study aimed to investigate whether time-restricted feeding (TRF) can reverse these obesity-associated immune disturbances.

In this study, we investigated the impact of TRF on microglial function in male Wistar rats fed either a standard chow diet or HFD. Food access was restricted to the dark phase (TRF dark-fed) or the light phase (TRF light-fed) and compared to those without any time restriction, i.e. *ad libitum*-fed. Sacrifices were performed every four hours over the 24-hour light/dark cycle. Subsequently, brains and peripheral blood mononuclear cells (PBMCs) were isolated. Brains were used to isolate microglia for RNA sequencing and to profile microglia at the morphological level (Fig. 1a).

Results

Metabolic effects of TRF under different dietary conditions.

In the standard chow diet condition, we observed that both TRF light- and TRF dark-fed reduced body weight gain in the second and third week compared to the *ad libitum* group. However, this impact diminished in the fourth week (Fig. 1b). This is explained by the *ad libitum*-fed rats consistently showing higher caloric intake during the first 3 weeks of the TRF period (Fig. 1c). Moreover, food efficiency showed a decrease over time in the *ad libitum* fed animals with higher food efficiency compared to the TRF groups in week 2 and 3 (Fig. 1d), in contrast, after an initial drop food efficiency increased in both TRF groups, with the TRF light-fed group displaying a significantly higher food efficiency in week 4 (Fig. 1d), indicating increased body weight gain with the same amount of food intake.

In the HFD condition, both light-fed and dark-fed led to lower body weight gain compared to the *ad libitum* feeding (Fig. 1e). Similar to chow-fed rats, HFD *ad libitum* rats exhibited increased food intake (Fig. 1f). In contrast to chow-fed rats, both the TRF light- and dark-fed group exhibited lower food intake and food efficiency compared to *ad libitum* during the entire experiment (Fig. 1f,g). HFD significantly increased relative fat mass in Wistar rats (Fig. 1h). No difference in adiposity was found between the three chow-fed groups (Fig. 1h). However, in the HFD condition the HFD dark-fed strategy resulted in lower body adiposity compared to both *ad libitum* and TRF light-fed (Fig. 1h). These results show that, even with an unhealthy diet, aligning the diurnal feeding period with the active phase can reduce adiposity.

TRF alters the transcript expression of microglial core clock gene.

In mammals, the molecular clock machinery exists in nearly every cell type [38], including the microglia [25]. In the standard chow as well as the HFD condition, most clock genes showed significant daily oscillations in the *ad libitum* and TRF dark-fed groups. The amplitude of *Nr1d1* and *Cry2* oscillation was higher in the HFD dark-fed group (Fig. 2a-b, 2d-e). In the TRF light-fed group, rhythmic expression was maintained in general, but the amplitude and acrophase of most clock gene oscillations were significantly altered compared to *ad libitum,* both in the chow and HFD conditions (Fig. 2c, 2f). Evaluation of the number of rhythmic genes in the different groups showed the following: 2,142 rhythmic genes in the chow *ad libitum*-fed group, 4,109 in the chow dark-fed group, 3,910 in the chow light-fed group; 3,805 in the HFD *ad libitum*-fed group, 4,623 in the HFD dark-fed group, and 1,770 in the HFD light-fed group (gene lists shown as deposit data). It is known that in obesity, PBMCs can infiltrate adipose tissue, leading to macrophage activation and increased pro-inflammatory activity [39-41]. In view of our observations in microglia, we were interested in whether the same effect could be seen in PBMCs in the systemic circulation. However, we didn't observe similar alterations in PBMCs as found in microglia, suggesting this is a microglia-specific response to TRF (Extended Fig. 1).

Microglial gene rhythmicity is highly sensitive in response to TRF.

To compare alterations in microglial transcriptional rhythmicity in rats under different feeding conditions we employed the CompareRhythm R package [42], which uses probability assignment to categorize rhythmicity alternations into ‘gain,’ ‘loss,’ or ‘shift’ rhythmicity, as well as identifying genes with 'unchanged' rhythmicity within a 24-hour timeframe (Fig. 3).

In the chow diet group, a large proportion of gene rhythms remained unchanged in the dark-fed group (Fig.3c), whereas in the light-fed group most genes gained rhythmicity in comparison to the chow *ad libitum* group (Fig.3a). Gene ontology (GO) analysis revealed that genes that gained rhythmicity were associated with microglia-mediated processes such as CNS development, cellular regulation, cytoskeleton organization, protein metabolism, response to stimulus and lipid metabolism (Extended Fig. 2a). Pathway analysis of the chow light-fed genes that gained rhythmicity showed enrichment in protein transport, catabolic process, endocytosis, autophagy and lipid metabolism (Extended Fig. 2c). The number of genes that gained rhythmicity was slightly higher in light-fed rats than in dark-fed rats (Fig. 3b, 3d). GO analysis showed that dark-fed genes with gained rhythmicity were mainly involved in cellular catabolic process, lipid metabolism and transport (Extended Fig. 2b). Pathway analysis of chow dark-fed with gained rhythmicity showed enrichment in lipid metabolism, amino acid metabolism, insulin signaling, chromatin organization, protein signaling and element-binding signaling (Extended Fig. 2d).

Both TRF groups show a clear adaptation to the time-restricted condition when on chow diet. We then examined the number of genes with the same rhythmic changes in light-fed and dark-fed rats, and identified 326 genes that gained rhythmicity in both the light-fed and dark-fed group, 110 genes that lost rhythmicity, and 14 genes with shifted rhythmicity in both TRF groups (Fig. 3e). Further enrichment analysis revealed that gene expressions with gained rhythmicity were primarily associated with protein and lipid metabolism and lysosomal functions (Fig. 3f), while genes that lost their rhythmicity were linked to transport (Fig. 3g).

HFD light-fed induced the most significant loss of rhythmicity in gene expression in microglia

Under HFD-feeding conditions, gene expressions that lost rhythmicity accounted for the largest proportion in the TRF light-fed group, constituting nearly 80% of the changes compared to the *ad libitum* group (Fig. 4a, 4b). GO analysis revealed the involvement of genes that lost rhythmicity with HFD light-fed in processes including cellular metabolic process, cell matrix, cell metabolism, protein metabolism, response to stimulus and signal transduction (Extended Fig. 2e). Pathway analysis showed mainly network enrichment in protein catabolic process, metabolism of RNA, cellular response to stress, ncRNA processing, nucleocytoplasmic transport, intracellular protein transport, cell cycle and RHO GTPase cycle (Extended Fig. 2g). These findings indicate a significant disruption

in the circadian control of microglial cells when hypercaloric food is combined with incorrect timing of eating.

However, in HFD dark-fed rats rhythmicity remained largely unchanged and 775 genes gained rhythmicity compared with the *ad libitum* condition (Fig. 4c, 4d). The GO analysis revealed those genes that gained rhythmicity to be involved in microglia-mediated CNS development, protein metabolism and transport (Extended Fig. 2f). Pathway analysis showed mainly network enrichment in neuron projection development, cellular matrix, microtube cytoskeleton organization, cytoskeleton organization, cell cycle, synaptic vesicle cycle, RHO GTPase cycle, EGF / EGFP signaling pathway, insulin signaling and cell projection (Extended Fig. 2h).
In the HFD condition, light-fed and dark-fed rats shared 391 genes with lost rhythmicity, whereas only 22 genes gained rhythmicity, and 2 with shifted rhythmicity compared to HFD *ad libitum* (Fig. 4e). Further enrichment analysis of the genes with lost rhythmicity showed their association with hormone response and protein metabolism (Fig. 4f). These findings suggest that changes in microglial gene rhythmicity in response to time-restricted feeding has major effects on cellular metabolic reprogramming.

When comparing the effects of light-fed and dark-fed in the two diet compositions (Extended Fig. 3), we observed that a large proportion of genes (~75%) lost rhythmicity in the HFD light-fed compared to chow light-fed group. We further applied the same methodology to compare rhythmicity in rats fed chow or HFD *ad libitum* (Fig. 4g, 4h). Of note, we found approximately 55% of oscillatory genes showed no changes, whereas the rest showed loss or gain of rhythmicity (Fig. 4g, 4h). The enriched pathway categories show that genes with lost rhythmicity were mainly involved in cellular organization, CNS develop, transport and immune response (Extended Fig. 4a), while genes with gained rhythmicity were mainly involved in protein metabolism (Extended Fig. 4b), and genes with unchanged rhythmicity were largely involved in cellular regulation, CNS develop, lipid metabolism, protein metabolism, transport and cellular catabolic process (Extended Fig. 4c).

TRF alters microglial number in the ARC.

The arcuate nucleus (ARC) of the hypothalamus plays a critical role in regulating systemic energy homeostasis [43]. When comparing rhythmicity between chow and HFD *ad libitum* groups, we noted that >700 genes gained rhythmicity under HFD conditions (Fig. 4h). Enriched pathway analysis of these genes that gained rhythmicity revealed connections to signal transduction, metabolism, and cell cycle regulation (Fig. 5a). Subsequently, we examined those alternations in gain, loss, shift, and unchanged categories between different group comparisons (Fig. 5b). We found that a group of genes, marked in light blue in the Sankey diagram (Fig. 5b), gained rhythicmicty in HFD *ad libitum* vs chow *ad libitum*, whereas they lost rhythm in HFD dark-fed compared to the HFD *ad libitum* group (Fig. 5b). Pathway enrichment analysis of these light blue-marked genes mainly revealed cell cycle-related

pathways (Fig. 5c). It is known that a high-fat diet significantly increases the number and ramifications of microglia in the hypothalamus compared with a chow diet [44, 45].

To further check microglial surveillance activity at the morphological level, we performed immunohistochemistry using an ionized calcium-binding adaptor molecule 1 (Iba1) marker (Fig. 5d). The obesogenic diet caused an increased microglial cell number and ramifications as compared to the chow *ad libitum* condition (Fig. 5e, f). Importantly, we found that this increase in the number of microglial cells was not observed in the HFD dark-fed group (Fig. 5e). This shows that the HFD-induced increase in microglial activity can be reversed by restricted-feeding in the dark period, which is the active period for these nocturnal rodents. Microglial immune surveillance and scavenging functions heavily depend on phagocytosis and lysosome activity [46]. We further examined genes associated with phagolysosome and immune response functions (Fig. 5g, 5h). Under chow conditions, the dark-fed group exhibited higher gene expressions related to immune response and phagolysosome activity at ZT14, whereas the light-fed group showed higher expressions at ZT2 compared to the *ad libitum*-fed group. In the HFD condition, these changes were less obvious in the dark-fed group; however, we observed that the light-fed group had increased gene expression in immune response and phagolysosome functions at ZT2 compared to the *ad libitum*-fed group.

Microglial morphological characteristics in other brain regions.

Our investigation also aimed to discern potential variations in microglial morphological characteristics across distinct brain regions, including the cortex, hippocampal CA1, thalamus and ventromedial nucleus of the hypothalamus (VMH) (Extended Fig. 5). Interestingly, we observed a common increase in the number of microglial cells in the HFD dark-fed group compared to the HFD *ad libitum* group at the beginning of the light phase in the cortex, hippocampal CA1, and thalamus regions (Extended Fig. 5b). This observation implies that the timing of feeding may affect microglial cell numbers differentially across various brain areas. We also found that HFD resulted in an overall increase in the number of microglial ramifications, which was not prevented by changes in (TRF-induced) feeding patterns (Extended Fig.5c). In the VMH, we noted a reduced number of microglial cells at the onset of the light period in the group subjected to HFD with light-fed compared to the *ad libitum* group.

HFD significantly impairs the elasticity of microglial pathways.

Through unsupervised gene set variation analysis (GSVA) combined with the Mfuzz time clustering method, we estimated the daily variation of pathway activity across the sample population and identified four distinct clusters (Extended Fig. 6a). Notably, the chow dark-fed group constituted the largest proportion of pathways in cluster 4 (with a peak at the onset of the dark period), comprising nearly 80% of the samples (gene lists shown as deposit data). We then studied variation in clusters among the three different feeding patterns, we found there was a clear transition from cluster 3 in the chow *ad libitum* group to cluster 4 (peak during the early dark phase) in the chow dark-fed group

239 (Extended Fig. 6c). Few shifts were observed from cluster 1-2 in the chow *ad libitum* group to cluster
240 1-3 in the chow light-fed group (Extended Fig. 6b). Further comparisons between the number in each
241 cluster under control and HFD conditions, revealed a significant reduction in pathway enrichment in
242 HFD compared to chow conditions (compare Extended Fig. 6a vs. 6d). While no cluster shifting was
243 observed between HFD *ad libitum* and light-fed groups (Extended Fig. 6e), some transitions were still
244 evident between HFD *ad libitum* and HFD *dark-fed* (Extended Fig. 6f), for instance from HFD *ad*
245 *libitum* cluster 1 to cluster 4 in HFD dark-fed, and from cluster 2 in HFD *ad libitum* to cluster 1 in HFD
246 dark-fed (Extended Fig. 6f).
247
248 **Impaired microglial immunometabolism induced by HFD cannot be rescued by TRF.**
249 The effectiveness of TRF during the active (dark) period in reducing adiposity (Fig. 1h) and microglial
250 number (Fig. 5e) indicated promising prospects for weight loss. However, TRF also poses significant
251 challenges, including limited weight loss outcomes over prolonged periods and difficulties in
252 sustaining weight loss in human trials [47, 48]. Recent insights suggesing enduring brain responses
253 after weight loss in formerly obese individuals [49], prompted us to investigate potential hardwired
254 characteristics of microglial genes.
255
256 Analysis via the Sankey diagram unveiled that genes that gained rhythmicity in both chow dark-fed
257 and HFD dark-fed compared to their own ad libitum control were mainly associated with cellular
258 energy metabolism pathways (the orange line in Fig. 6a). It's known that microglial function heavily
259 relies on metabolic adaptability (encompassing glycolysis, oxidative phosphorylation, lipid metabolism,
260 and amino acid metabolism), facilitating swift shifts in energy utilization between resting and active
261 states [33, 46]. In the chow condition, metabolism-related genes showed a pronounced expression
262 during the dark period in the dark-fed group, this was less clear in the chow light-fed group (Fig. 6b-f).
263 However, the chow light-fed group had a clear reversed day-night expression compared to normal
264 chow ad libitum in glycosis and arginine metabolism, with notobaly higher expression during light
265 phase and lower expression duing dark-phase (Fig. 6c, 6d). Moreover, HFD accentuated microglial
266 lipogenesis, lipid droplets (LDs) biogenesis and lipid uptake and transport in lipid metabolism (Fig. 6b),
267 while glycolysis, arginine metabolism, lipolysis and the electron transport chain were significantly
268 suppressed compared to the chow condition (Fig.6c-e). Surprisingly, neither the light-fed nor dark-fed
269 strategies were able to reverse the metabolic changes induced by the HFD (Fig. 6b-f). Mitochondria
270 are essential for microglial metabolism and death, and their functions are controlled by their dynamics,
271 including fission/fusion [50-52]. TRF didn't significiantly alter microglial mitochondrial dynamics.
272 Collectively, these data show that while TRF modulates microglial immune responses to a high-fat diet,
273 the detrimental effects of a high-fat diet on microglial metabolism persist.
274
275 TOM20 is one of the receptor systems of the translocase of the outer membrane (TOM) complex in
276 the outer mitochondrial membrane and is encoded by the TOMM20 gene. To further determine cell-
277 type-specific mitochondrial alterations, we colocalized TOOM20 with IBA1 or NeuroTrace to identity
278 the mitochondria in microglia and neurons (Fig,7a,7b). Tomm20 expression in microglia was

279 significantly increased in the HFD light- and dark-fed groups compared to the chow ligh- and dark-fed
280 groups (Fig. 7c). Although there were no significant changes in the volume of the TOMM20 protein in
281 neurons of TRFs, at ZT6 their volume was significantly higher in HFD *ad libitum* compared to chow *ad*
282 *libitum* (Fig. 7d). We also investigated the spatial relationship between neurons and microglia across
283 the circadian cycle. In the chow diet group, microglia were found to be in closer proximity to neurons
284 during the night compared to the day, indicating a circadian modulation of neuron-microglia
285 interactions (Fig. 7e). However, in the HFD group, this circadian variation in microglial-neuronal
286 contact was absent, with microglia consistently maintaining close proximity to neurons, irrespective of
287 the time of day (Fig. 7f). The time-restricted feeding (TRF) intervention did not significantly alter the
288 baseline neuron-microglia interaction patterns observed in either the chow or HFD groups (Fig.7e, 7f).
289 Taken together, these findings suggest that although the volume of microglial mitochondria increased
290 in the HFD groups compared to the chow groups, their functionality remains impaired. The inability of
291 TRF to reverse the detrimental metabolic changes induced by a high-fat diet, especially in microglial
292 mitochondrial activity, highlights a persistent state of metabolic and mitochondrial dysregulation.
293
294 **Discussion**
295 Our study aimed to elucidate the impact of time-restricted feeding on the complicated relation
296 between the microglial circadian clock and diet. We found that adoption of a time-restricted feeding
297 strategy has beneficial effects on body composition and microglial rhythmicity. However, the
298 detrimental effects of an HFD on immunometabolism could not be reversed by time-restricted feeding.
299
300 In the presence of *ad libitum* access to food, HFD impairs circadian feeding rhythms more severely
301 than does a standard chow diet [7, 53]. Therefore, rodents fed HFD *ad libitum* have a short fasting
302 period and a long feeding window [5]. Such eating patterns disrupt circadian rhythms and the
303 metabolic pathways that are coupled with the daily feeding rhythm. Emerging ideas suggest that TRF
304 may contribute to beneficial metabolic outputs [5, 54]. In the HFD condition, we found that TRF light-
305 and dark-feeding cause similar alterations in body weight gain, weekly food intake, and weekly food
306 efficiency. However, relative fat mass was only reduced in HFD dark-fed rats compared to HFD *ad*
307 *libitum*, not in the HFD light-fed group. This suggests that the timing of food intake during the active
308 period, thus aligned with the day-night rhythm, has a positive impact on body composition
309 independent of calorie restriction *per se*. Our observation is supported by studies showing that HFD
310 dark-fed mice had increased ghrelin and leptin effectiveness [55, 56], thereby contributing to less
311 adiposity. Hence, the timing of food intake emerges as an important factor influencing body
312 composition and metabolic outcomes.
313
314 Circadian rhythms and the immune system are fundamentally linked, as evidenced by the fact that
315 they are both subject to the same fundamental biological processes [25, 26]. Indeed, the majority of
316 cells within the immune system exhibit autonomous circadian oscillations in gene expression.
317 Moreover, core clock genes regulate key immune transcription factors that drive rhythmic expression
318 of cytokines and the function of immune receptors [26-31] and circadian proteins regulate

inflammatory responses, immune cell trafficking, and phenotype [28, 29, 31-34]. Beyond light exposure, also the timing of food intake influences circadian rhythms. For instance, timed feeding entrains rhythmic clock gene expression in the suprachiasmatic nucleus of mice kept in constant darkness and restores rhythmicity in mice kept in constant light [57, 58]. The circadian timing system is an internal timekeeping system that coordinates physiological processes and hormonal release patterns in accordance with day/night cycles in behavior [59, 60]. Previously wer found that deletion of the core circadian clock gene *Bmal1* in a microglia-specific manner protects mice from high fat diet-induced obesity [61]. In the current study we found that microglial clock gene expression is highly sensitive to time-restricted feeding, while no significant effects were seen on monocyte circadian gene expression. A potential explanation for this discrepancy between two closely related cell types may be the blood–brain barrier, a morpho-functional structure that separates the CNS from the circulation [62]. Another possible explanation is the longevity and self-renewal capacity of microglia, which differs markedly from that of PBMCs [63, 64]. Microglia are known to have a substantially longer lifespan and possess the ability to self-renew. The lifespan of human microglia is on average 4.2 years [63, 64], while PBMCs have a relatively short lifespan, typically lasting from a few days to a few weeks [65]. Therefore, the absence of clear TRF-induced alterations in PBMCs may be explained by their faster turnover and shorter lifespan.

The basic paradigm of circadian regulation of metabolism is that rhythmic patterns of gene expression drive rhythms in cellular metabolism [5, 8]. TRF is known to further increase the number of rhythmic transcripts in WT mice fed a normal chow diet [5]. In the chow condition, we observed that in light-fed rats a similar number of genes gained rhythmicity compared to dark-fed rats. While most of the clock gene rhythms remained unchanged, in chow light-fed group also a considerable number of genes lost rhythmicity. This part of the data indicates there is a strong capacity of the microglial instrinsic clock to adapt to feeding cues [66]. However, in the HFD condition, we observed a clear enhanced expression of genes involved in lipogenesis and LDs biogenesis together with decreased expression of genes involved in glycosis, arginine metabolism, lipolysis and electron transport chain. Since the rhythm of most core clock genes remained unchanged, this suggests that the greater effect of TRF on microglia lies in the absolute level of expression rather than its temporal profile.

Although feeding restricted to the dark period failed to rescue the HFD-induced downregulation of certain metabolism-related pathways, a more robust day-night difference when compared to the HFD *ad libitum* and light-fed groups, especially in electron transport chain (ETC), is still evident. Although HFD dark-feeding successfully rescued the loss of rhythmicity in some metabolism-related pathways, we did not see a reinstatement of gene expression levels in the ETC. This part of the data indicated that microglial transcription regulation is mostly affected by (micro)environmental cues rather than microglial instrinsic clock modulation.

During inflammation, microglial priming suggests that microglia exhibit heightened reactivity when faced with a second stimulus compared to those without prior stimulation [67-69]. This phenomenon

implies a form of "microglial memory" that amplifies the response to subsequent similar stimulus [67-69]. However, it's not fully understood whether also a memory exists at the immunometabolic level, involving the interaction between metabolism and the immune response. Our data indicate a potential "obesogenic memory" in microglia, as the metabolic impairment induced by HFD intake persists despite either light or dark time-restricted feeding. This observation suggests two potential interpretations: either microglial priming is facilitated by epigenetic alterations [70], or a microglial memory that is stored elsewhere within the neural or glial network. For instance, it has been shown that a persistent elevation of microglial reactivity and consequent TNFα secretion induces mitochondrial stress in POMC neurons, which contributes to the development of obesity [45].

In summary, our study revealed that 4 weeks of time-restricted feeding during the active phase of the light/dark cycle effectively decreased the fat gain induced by a high-fat diet. However, the HFD-induced impaired cellular metabolic changes in microglia persisted. The "obesogenic memory" in microglia we defined suggests a potential explanation for the weight cycling effect, *i.e.* the repeated loss and regain of weight loss often seen during dieting and also known as the "yo-yo" effect [71, 72]. We think this newly defined concept of 'microglial obesogenic memory' prompts a re-evaluation of microglial functions in both health and disease contexts. The effectiveness of long-term TRF in eliminating obesity memory in microglia remains unknown and needs further investigation. Furthermore, the precise dynamics of microglial mitochondrial function and regulation during different diet and circadian conditions is unknown, and further studies are needed to investigate these mechanisms and their relevance to human conditions. However, despite these limitations, we think our findings have significant translational implications and suggest that combining appropriately timed restricted feeding with immunological considerations may improve weight loss treatment.

Data availability

All data associated with this study are present in the paper or the Supplementary Materials. Any additional information required to reanalyze the data reported here is available from the corresponding authors upon reasonable request.

Code availability

All codes used in the current study are available via GitHub (https://github.com/NeuroAnalyz/SpikeTrains-LFP) or from the corresponding authors upon reasonable request.

Acknowledgments

We would like to thank Aldo Jongejan and Perry Moerland from the Bioinformatics Unit for help and advice. We are also grateful to Richard Volckmann from the R2 Genomics Platform for assistance and discussions.

Funding

This study was sponsored by the Netherlands-Canada Type 2 Diabetes Research Consortium. H.J. is financially supported by the CSC (China Scholarship Council).

Declaration of interests

The authors declare no competing interests.

Material and methods

Animals

Male Wistar rats (n = 293) (Charles River Laboratories, Sulzfeld, Germany) were group-housed in a 12h-12h light-dark (LD) or reversed 12h-12h dark-light (DL) cycle with light on or off at 07:00 and 19:00 [with lights on defined as Zeitgeber Time zero (ZT0) and lights off as ZT12] and a room temperature of 22 ± 2°C. Upon arrival, animals received a standard chow diet (2018, Teklad diets, Invigo) or an obesogenic diet (D12331, Research Diets Inc). During an acclimatization period of 4 weeks, animals had *ad libitum* access to food and water. Animals were group-housed in different batches for logistic reasons. After the 4-week acclimatization period, animals receiving the same diet were randomized based on their body weight and the time-restricted feeding protocol was started. Animals in the LD room received light-phase feeding (10 hours of feeding from ZT1-ZT11) and animals in the DL room dark-phase feeding (10 hours of feeding from ZT13-ZT23). Animals fed *ad libitum* were randomized between the normal LD and reversed DL conditions. Body weight and food intake were monitored twice per week. Body composition of all animals was measured by MRI in the last week. All studies were approved by the Animal Ethics Committee of the Royal Dutch Academy of Arts and Sciences and performed according to the guidelines on animal experimentation of the Netherlands Institute for Neuroscience.

Tissue sampling

After 4 weeks of TRF, animals were sacrificed at six different time points during the 24-hour day-night cycle (starting at ZT2, every four hours) by euthanasia with 60% CO_2/40% O_2, followed by decapitation. Trunk blood was collected, and the brain was isolated and dissected as described earlier [73]. One half of the forebrain was immediately stored in 4% PFA for 48 hours and transferred to 1x PBS containing 0.05% sodium azide (NaN_3) for further analysis. From the other half of the forebrain, the hypothalamus and hippocampus were extracted, immediately frozen in liquid nitrogen and stored at -80°C for further analyses.

Immunohistochemistry and Immunofluorescence

After 48 hours post-fixation the brains were equilibrated in a 30% sucrose solution. Coronal sections of the brains, with a thickness of 30 µm, were obtained using a cryostat (Leica Biosystems). These sections were collected and rinsed in 0.1 M Tris-buffered saline (TBS) to ensure proper tissue preparation.

436 Immunohistochemical staining was performed to detect the presence of Iba1 in the brain. Sections
437 were incubated with a primary antibody, rabbit anti-Iba1 (1:1000, Synaptic Systems, No.234003,
438 Germany). The primary antibodies were incubated overnight at 4 °C. Following rinsing, the sections
439 were incubated with biotinylated secondary antibody, goat anti-rabbit IgG (1:400, BA-1000, Vector
440 Laboratories, Inc., Burlingame, CA), and then further incubated in avidin-biotin complex (1:800, PK-
441 4000, Vector Laboratories, Inc., Burlingame, CA) for 1 hour. The reaction product was visualized by
442 incubating the sections in a solution of 1% diaminobenzidine with 0.01% hydrogen peroxide for
443 10 minutes. Subsequently, the sections were mounted on slides, dried, dehydrated through a graded
444 series of ethanol, cleared in xylene, and coverslipped for image collection and quantification.
445 Images were acquired using a Zeiss AXIO Scope A1 microscope equipped with Plan-APOCHROMAT
446 × 10/0.45 objective lenses and a Zeiss AxioCam MRc camera. AxioRel Vision 4.8 acquisition software
447 was used for image capture. Quantification of imaging data was carried out in a blinded manner,
448 where Iba1-immunoreactive (Iba1-ir) cell numbers and processes were manually counted. For
449 immunofluorescence staining, fluorescent-conjugated antibodies Guinea pig anti-IBA1 (1:500, ,
450 Synaptic System, No. 234 308), Rabbit anti-TOMM20 (1:500, Proteintech, 11802-1-AP) were added.
451 After several rinses, brain sections were mounted on Superfrost Plus microscope slides, covered with
452 cover slips, and stored at 4°C. Imaging was performed using a confocal microscope (TCS-SP8, Leica
453 Biosystems, Heidelberg, Germany). The laser power, photomultiplier gain, and offset were maintained
454 constant for all images.
455
456 **Blood mononuclear myeloid isolation and plasma collection**
457 Trunk blood was used for monocyte isolation and plasma collection. For plasma collection, 2 ml blood
458 was centrifuged for 15 min (4,000 rpm, 4°C, break 9/9). Plasma was collected and stored at −20°C
459 until further analyses. For monocyte isolation, 30 ml lysis buffer (containing 1 × ACK; 155 mM NH4Cl;
460 10 mM KHCO3; 0.1 mM EDTA) was added to ~3 ml blood, mixed by gently vortexing and incubated at
461 RT for 10–15 min. Cell suspension was centrifuged for 5 min (200 g, RT, break 9/9). Supernatant was
462 discarded and cells were resuspended in 2 ml PBS-FBS (PBS containing 1% FBS). After
463 centrifugation of the new cell suspension for 5 min (200 g, RT, break 9/9), supernatant was discarded,
464 and cells were resuspended in 0.5 ml PBS-FBS. The obtained cell suspension was added to 4.5 ml
465 RPMI medium and slowly layered on 5 ml Ficoll® (17-1440-02, GE Healthcare, Sigma-Aldrich®) in a
466 15 ml Falcon tube, followed by centrifugation for 30 min (400 g, 20°C, break 1/1). The fuse interphase,
467 containing monocytes, was collected in 8 ml 1x HBSS, and centrifuged for 5 min (200 g, RT).
468 Supernatant was discarded and the monocyte pellet was resuspended in RNA Lysis buffer (Qiagen)
469 and stored at -80°C until RNA extraction.
470
471 **RNA isolation from isolated PBMCs and quantitative reverse-transcription polymerase chain**
472 **reaction**
473 Total RNA was isolated from PBMCs using a RNeasy Micro Kit (QIAGEN, Hilden, Germany, cat. no.
474 74004) following the manufacturer's recommendations. We used 250 ng of monocyte RNA to
475 generate cDNA with a Transcriptor First Strand cDNA Synthesis Kit (Roche, Basel, Switzerland, cat.

476 no. 04897030001) following the manufacturer's instructions. Quantitative PCR (qPCR) was performed
477 using a SensiFAST™ SYBR® No-ROX Kit (Roche Bioline, cat. no. BIO-98020). Expression levels of
478 all genes were normalized to the geometric mean of housekeeping genes. Primer sequences (see
479 Table S1) were designed using the Basic Local Alignment Search Tool (BLAST) from the National
480 Center for Biotechnology Information (NCBI). Primers were purchased from Sigma-Aldrich® and
481 validated by melt curve analysis and DNA band size and/or purity on agarose gel electrophoresis
482 (data not shown).

Genes	Primer sequence - Forward	Primer sequence - Reverse
Arntl	CCGATGACGAACTGAAACACCT	TGCAGTGTCCGAGGAAGATAGC
Clock	CGATCACAGCCCAACTCCTT	TTGCAGCTTGAGACATCGCT
Nr1d1	AAGACCTTACTGCTCGGTGC	TGTAGGTGATAACACCACCTGT
Dbp	CCTTTGAACCTGATCCGGCT	TGCCTTCTTCATGATTGGCTG
Per1	TGGGGGCCAAGAAAGATACG	CACCACGCTCTCTGCCTTAT
Per2	CACCCTGAAAAGAAAGTGCGA	CAACGCCAAGGAGCTCAAGT
Cry1	AAGTCATCGTGCGCATTTCA	TCATCATGGTCGTCGGACAGA
Cry2	GTTTGACCGAATGGAGGGGA	AGCAACTCATCAAATACCCGGA
Rpl13a	CTGCCGAAGATGGCGGAGGG	CACCTTTCGGCCCAGCAGTACCT
Actb	ACAACCTTCTTGCAGCTCCTC	CTGACCCATACCCACCATCAC
Hprt	TTGGTCAAGCAGTACAGCCC	CTTGCCGCTGTCTTTTAGGC

483 Table S1. Primer sequences of target genes.
484
485 **Microglia isolation**
486 Percoll isopycnic isolation was performed to isolate microglial cells from the cerebral brain cortex and
487 one half of the midbrain without the hippocampus and hypothalamus. Briefly, brains were
488 mechanically homogenized with RPMI 1640 medium (11875-093, Gibco™) using a tissue grinder
489 (Mexico, Sigma-Aldrich), after which the brain homogenate was filtered through a 70 µm cell strainer
490 (431751, Corning®) in a 50 ml Falcon tube. The filtered brain homogenate was centrifuged for 5 min
491 (380 g, 4°C, break 9/9). Supernatant was discarded and pellet was resuspended in 7 ml RPMI
492 medium and mixed with 100% Percoll solution [for 10 ml: 9 ml Percoll® stock (17-5445-01, GE
493 Healthcare, Sigma-Aldrich®) together with 1 ml 10x HBSS (14185-045, Gibco™)]. The cell
494 suspension was slowly layered on 70% Percoll solution [for 10 ml: 7 ml 100% Percoll solution with 3
495 ml 1x HBSS (14175-053, Gibco™)] in a 15 ml Falcon tube and centrifuged for 30 min (500 g, 18°C,
496 break 1/0). Myelin and cell debris were discarded and the fuse interphase, containing microglial cells,
497 was carefully collected in 8 ml 1x HBSS, followed by centrifuging for 7 min (500 g, 18°C, break 9/9).
498 Supernatant was discarded and the microglial cell pellet was resuspended in RNA Lysis buffer
499 (Qiagen) and stored at -80°C until RNA extraction.
500
501 **Microglial RNA sequencing**
502 To study differences in microglial gene expression, RNA sequencing was performed. RNA from
503 microglial cells was isolated using the RNeasy Micro Kit (Qiagen), according to the manufacturer's

guidelines. mRNA was enriched from total RNA with the Dynabeads® mRNA Purification Kit (61006, Invitrogen). A strand-specific transcriptome library was constructed using the MGIEasy RNA Directional Library Prep Set (16 RXN) (1000006385, MGI). Briefly, after cDNA synthesis, adaptor ligation was performed to ligate adaptors with the cDNAs. Subsequently, a PCR reaction was conducted to amplify the cDNAs, after which the library quality was checked using the Agilent 2100 Bioanalyzer (G2939AA, Agilent). Finally, single-stranded cyclized products were produced from single-stranded PCR products. To perform sequencing, single-stranded circle DNA molecules were replicated via rolling cycle amplification and a DNA nanoball (DNB) was generated. Sequencing was performed through combinatorial Probe-Anchor Synthesis (cPAS) on the DNBSEQ-G400 (G400, MGI).

Statistical analyses

Data are expressed as mean ± SEM. Two-way ANOVA with multiple comparisons was used to compare multiple groups at each weekly time point throughout the TRF period and at each ZT throughout the 24-hour day-night cycle. $P < 0.05$ was considered to be statistically significant. Statistical analyses were performed using GraphPad Prism (v 9.5.1).

Sequencing data was filtered using SOAPnuke [74] by (1) Removing reads containing sequencing adapter; (2) Removing reads whose low-quality base ratio (base quality less than or equal to 15) is more than 20%; (3) Removing reads whose unknown base ('N' base) ratio is more than 5%, afterwards clean reads were obtained and stored in FASTQ format. Clean sequence reads were aligned to the reference genome (Rattus_norvegicus, GCF_000001895.5_Rnor_6.0) using HISAT2 [75], after which Ericscript (v0.5.5) [76] and rMATS (V3.2.5) [77] were used to detect fusion genes and differential splicing genes (DSGs), respectively. Clean sequence reads were aligned to a reference gene set, a database built by the Beijing Genomic Institute in Shenzhen (BGI), in which known and novel coding and non-coding transcripts were included, using Bowtie2 [78]. Raw counts matrix was normalized by transcripts per million (TPM). We performed rhythm analysis using cosinorPy(v2.1) [79], JTK_CYCLE and compareRhythm(v1.0.1) [42]. We described the circadian rhythmicity of genes within each group using 1 component trigonometric regression model using cosinor.fit_group in CosinorPy. The mean expression of each group was calculated for circadian comparison among groups and genes with mean expression less than 5.5 in each group were filtered. We applied model selection methods in compareRhythm using the Bayesian information criterion. Comparison of the amplitude (one-half the peak-to-trough difference) and acrophase (the peak time of the fitted curve) of selected genes among the groups was performed using cosinor1.test_cosinor_pairs.

We applied GSVA (v1.48.3) [80] to estimate the variation of pathway activity within each group using the Poisson kernel. The canonical pathways gene sets were downloaded from the Molecular Signatures Database (MSigDB, https://www.gsea-msigdb.org/gsea/msigdb). Pathways were clustered using Mfuzz(v2.60.0) [81] according to their expression change over time and Metascape [http://metascape.org] web-based tool. CompareRhythms was also performed to detect the rhythm of pathways. The chord plot generated by circlize (v0.4.15) and the pathways network plot generated by igraph (v1.5.1). The Sankey plot was generated by ggsankey (v 0.0.99999).

544 ## References

545 1. *Worldwide trends in body-mass index, underweight, overweight, and obesity from 1975 to*
546 *2016: a pooled analysis of 2416 population-based measurement studies in 128·9 million*
547 *children, adolescents, and adults.* Lancet, 2017. **390**(10113): p. 2627-2642.
548 2. *Global, regional, and national burden of diabetes from 1990 to 2021, with projections of*
549 *prevalence to 2050: a systematic analysis for the Global Burden of Disease Study 2021.*
550 Lancet, 2023. **402**(10397): p. 203-234.
551 3. Blüher, M., *Obesity: global epidemiology and pathogenesis.* Nat Rev Endocrinol, 2019. **15**(5):
552 p. 288-298.
553 4. Gill, S. and S. Panda, *A Smartphone App Reveals Erratic Diurnal Eating Patterns in Humans*
554 *that Can Be Modulated for Health Benefits.* Cell Metab, 2015. **22**(5): p. 789-98.
555 5. Hatori, M., et al., *Time-restricted feeding without reducing caloric intake prevents metabolic*
556 *diseases in mice fed a high-fat diet.* Cell Metab, 2012. **15**(6): p. 848-60.
557 6. Sherman, H., et al., *Timed high-fat diet resets circadian metabolism and prevents obesity.*
558 FASEB J, 2012. **26**(8): p. 3493-502.
559 7. Kohsaka, A., et al., *High-fat diet disrupts behavioral and molecular circadian rhythms in mice.*
560 Cell Metab, 2007. **6**(5): p. 414-21.
561 8. Chaix, A., et al., *Time-Restricted Feeding Prevents Obesity and Metabolic Syndrome in Mice*
562 *Lacking a Circadian Clock.* Cell Metab, 2019. **29**(2): p. 303-319 e4.
563 9. Chaix, A., et al., *Time-restricted feeding is a preventative and therapeutic intervention*
564 *against diverse nutritional challenges.* Cell Metab, 2014. **20**(6): p. 991-1005.
565 10. Reid, K.J., K.G. Baron, and P.C. Zee, *Meal timing influences daily caloric intake in healthy*
566 *adults.* Nutr Res, 2014. **34**(11): p. 930-5.
567 11. Regmi, P. and L.K. Heilbronn, *Time-restricted eating: benefits, mechanisms, and challenges in*
568 *translation.* Iscience, 2020. **23**(6).
569 12. Chow, L.S., et al., *Time-Restricted Eating Effects on Body Composition and Metabolic*
570 *Measures in Humans who are Overweight: A Feasibility Study.* Obesity (Silver Spring), 2020.
571 **28**(5): p. 860-869.
572 13. Rothschild, J., et al., *Time-restricted feeding and risk of metabolic disease: a review of human*
573 *and animal studies.* Nutrition reviews, 2014. **72**(5): p. 308-318.
574 14. Zarrinpar, A., A. Chaix, and S. Panda, *Daily Eating Patterns and Their Impact on Health and*
575 *Disease.* Trends Endocrinol Metab, 2016. **27**(2): p. 69-83.
576 15. Guerrero-Vargas, N.N., et al., *Time-restricted feeding prevents depressive-like and anxiety-*
577 *like behaviors in male rats exposed to an experimental model of shift-work.* J Neurosci Res,
578 2021. **99**(2): p. 604-620.
579 16. Chaput, J.-P., et al., *The role of insufficient sleep and circadian misalignment in obesity.*
580 Nature Reviews Endocrinology, 2023. **19**(2): p. 82-97.
581 17. Zeb, F., et al., *Effect of time-restricted feeding on metabolic risk and circadian rhythm*
582 *associated with gut microbiome in healthy males.* British Journal of Nutrition, 2020. **123**(11):
583 p. 1216-1226.
584 18. Valdearcos, M., et al., *Microglia dictate the impact of saturated fat consumption on*
585 *hypothalamic inflammation and neuronal function.* Cell Rep, 2014. **9**(6): p. 2124-38.
586 19. Valdearcos, M., et al., *Microglial Inflammatory Signaling Orchestrates the Hypothalamic*
587 *Immune Response to Dietary Excess and Mediates Obesity Susceptibility.* Cell Metab, 2017.
588 **26**(1): p. 185-197.e3.
589 20. Sugiyama, M., et al., *Hypothalamic glial cells isolated by MACS reveal that microglia and*
590 *astrocytes induce hypothalamic inflammation via different processes under high-fat diet*
591 *conditions.* Neurochem Int, 2020. **136**: p. 104733.
592 21. Baufeld, C., et al., *High-fat diet-induced brain region-specific phenotypic spectrum of CNS*
593 *resident microglia.* Acta Neuropathol, 2016. **132**(3): p. 361-75.

22. Mariani, M.M. and T. Kielian, *Microglia in infectious diseases of the central nervous system.* J Neuroimmune Pharmacol, 2009. **4**(4): p. 448-61.
23. Yang, I., et al., *The role of microglia in central nervous system immunity and glioma immunology.* J Clin Neurosci, 2010. **17**(1): p. 6-10.
24. Folick, A., S.K. Koliwad, and M. Valdearcos, *Microglial Lipid Biology in the Hypothalamic Regulation of Metabolic Homeostasis.* Front Endocrinol (Lausanne), 2021. **12**: p. 668396.
25. Fonken, L.K., et al., *Microglia inflammatory responses are controlled by an intrinsic circadian clock.* Brain Behav Immun, 2015. **45**: p. 171-9.
26. Keller, M., et al., *A circadian clock in macrophages controls inflammatory immune responses.* Proc Natl Acad Sci U S A, 2009. **106**(50): p. 21407-12.
27. Silver, A.C., et al., *The circadian clock controls toll-like receptor 9-mediated innate and adaptive immunity.* Immunity, 2012. **36**(2): p. 251-61.
28. Sato, S., et al., *A circadian clock gene, Rev-erbalpha, modulates the inflammatory function of macrophages through the negative regulation of Ccl2 expression.* J Immunol, 2014. **192**(1): p. 407-17.
29. Narasimamurthy, R., et al., *Circadian clock protein cryptochrome regulates the expression of proinflammatory cytokines.* Proc Natl Acad Sci U S A, 2012. **109**(31): p. 12662-7.
30. Arjona, A. and D.K. Sarkar, *Circadian oscillations of clock genes, cytolytic factors, and cytokines in rat NK cells.* J Immunol, 2005. **174**(12): p. 7618-24.
31. Scheiermann, C., Y. Kunisaki, and P.S. Frenette, *Circadian control of the immune system.* Nat Rev Immunol, 2013. **13**(3): p. 190-8.
32. Arjona, A. and D.K. Sarkar, *Evidence supporting a circadian control of natural killer cell function.* Brain Behav Immun, 2006. **20**(5): p. 469-76.
33. Gibbs, J.E., et al., *The nuclear receptor REV-ERBalpha mediates circadian regulation of innate immunity through selective regulation of inflammatory cytokines.* Proc Natl Acad Sci U S A, 2012. **109**(2): p. 582-7.
34. Nguyen, K.D., et al., *Circadian gene Bmal1 regulates diurnal oscillations of Ly6C(hi) inflammatory monocytes.* Science, 2013. **341**(6153): p. 1483-8.
35. Milanova, I.V., et al., *Diet-Induced Obesity Disturbs Microglial Immunometabolism in a Time-of-Day Manner.* Front Endocrinol (Lausanne), 2019. **10**: p. 424.
36. Yi, C.X., et al., *TNFalpha drives mitochondrial stress in POMC neurons in obesity.* Nat Commun, 2017. **8**: p. 15143.
37. la Fleur, S.E., et al., *The snacking rat as model of human obesity: effects of a free-choice high-fat high-sugar diet on meal patterns.* Int J Obes (Lond), 2014. **38**(5): p. 643-9.
38. Stenvers, D.J., et al., *Circadian clocks and insulin resistance.* Nat Rev Endocrinol, 2019. **15**(2): p. 75-89.
39. Xu, H., et al., *Chronic inflammation in fat plays a crucial role in the development of obesity-related insulin resistance.* J Clin Invest, 2003. **112**(12): p. 1821-30.
40. Ghanim, H., et al., *Circulating mononuclear cells in the obese are in a proinflammatory state.* Circulation, 2004. **110**(12): p. 1564-71.
41. Krinninger, P., et al., *Peripheral monocytes of obese women display increased chemokine receptor expression and migration capacity.* J Clin Endocrinol Metab, 2014. **99**(7): p. 2500-9.
42. Pelikan, A., et al., *Venn diagram analysis overestimates the extent of circadian rhythm reprogramming.* FEBS J, 2022. **289**(21): p. 6605-6621.
43. Morton, G.J., et al., *Central nervous system control of food intake and body weight.* Nature, 2006. **443**(7109): p. 289-95.
44. Gao, Y., et al., *Hormones and diet, but not body weight, control hypothalamic microglial activity.* Glia, 2014. **62**(1): p. 17-25.
45. Yi, C.X., et al., *TNFα drives mitochondrial stress in POMC neurons in obesity.* Nat Commun, 2017. **8**: p. 15143.

644 46. Colonna, M. and O. Butovsky, *Microglia Function in the Central Nervous System During*
645 *Health and Neurodegeneration.* Annu Rev Immunol, 2017. **35**: p. 441-468.
646 47. Liu, D., et al., *Calorie restriction with or without time-restricted eating in weight loss.* New
647 England Journal of Medicine, 2022. **386**(16): p. 1495-1504.
648 48. Hall, K.D. and S. Kahan, *Maintenance of Lost Weight and Long-Term Management of Obesity.*
649 Med Clin North Am, 2018. **102**(1): p. 183-197.
650 49. van Galen, K.A., et al., *Brain responses to nutrients are severely impaired and not reversed by*
651 *weight loss in humans with obesity: a randomized crossover study.* Nat Metab, 2023. **5**(6): p.
652 1059-1072.
653 50. Katoh, M., et al., *Polymorphic regulation of mitochondrial fission and fusion modifies*
654 *phenotypes of microglia in neuroinflammation.* Sci Rep, 2017. **7**(1): p. 4942.
655 51. Nunnari, J. and A. Suomalainen, *Mitochondria: in sickness and in health.* Cell, 2012. **148**(6): p.
656 1145-59.
657 52. Westermann, B., *Mitochondrial fusion and fission in cell life and death.* Nat Rev Mol Cell Biol,
658 2010. **11**(12): p. 872-84.
659 53. Pendergast, J.S., et al., *High-fat diet acutely affects circadian organisation and eating*
660 *behavior.* Eur J Neurosci, 2013. **37**(8): p. 1350-6.
661 54. Whittaker, D.S., et al., *Circadian modulation by time-restricted feeding rescues brain*
662 *pathology and improves memory in mouse models of Alzheimer's disease.* Cell Metab, 2023.
663 **35**(10): p. 1704-1721 e6.
664 55. Sorrell, J., et al., *The central melanocortin system mediates the benefits of time-restricted*
665 *feeding on energy balance.* Physiol Behav, 2020. **227**: p. 113132.
666 56. Briggs, D.I., et al., *Diet-induced obesity causes ghrelin resistance in arcuate NPY/AgRP*
667 *neurons.* Endocrinology, 2010. **151**(10): p. 4745-55.
668 57. Lamont, E.W., et al., *Daily restricted feeding rescues a rhythm of period2 expression in the*
669 *arrhythmic suprachiasmatic nucleus.* Neuroscience, 2005. **132**(2): p. 245-8.
670 58. Castillo, M.R., et al., *Entrainment of the master circadian clock by scheduled feeding.* Am J
671 Physiol Regul Integr Comp Physiol, 2004. **287**(3): p. R551-5.
672 59. Gerstner, J.R. and J.C. Yin, *Circadian rhythms and memory formation.* Nat Rev Neurosci,
673 2010. **11**(8): p. 577-88.
674 60. Man, K., A. Loudon, and A. Chawla, *Immunity around the clock.* Science, 2016. **354**(6315): p.
675 999-1003.
676 61. Wang, X.L., et al., *Microglia-specific knock-down of Bmal1 improves memory and protects*
677 *mice from high fat diet-induced obesity.* Mol Psychiatry, 2021. **26**(11): p. 6336-6349.
678 62. Cuddapah, V.A., S.L. Zhang, and A. Sehgal, *Regulation of the Blood-Brain Barrier by Circadian*
679 *Rhythms and Sleep.* Trends Neurosci, 2019. **42**(7): p. 500-510.
680 63. Reu, P., et al., *The Lifespan and Turnover of Microglia in the Human Brain.* Cell Rep, 2017.
681 **20**(4): p. 779-784.
682 64. Askew, K., et al., *Coupled Proliferation and Apoptosis Maintain the Rapid Turnover of*
683 *Microglia in the Adult Brain.* Cell Rep, 2017. **18**(2): p. 391-405.
684 65. Patel, A.A., et al., *The fate and lifespan of human monocyte subsets in steady state and*
685 *systemic inflammation.* J Exp Med, 2017. **214**(7): p. 1913-1923.
686 66. Guzman-Ruiz, M.A., et al., *Circadian modulation of microglial physiological processes and*
687 *immune responses.* Glia, 2023. **71**(2): p. 155-167.
688 67. Bilbo, S.D. and J.M. Schwarz, *Early-life programming of later-life brain and behavior: a critical*
689 *role for the immune system.* Front Behav Neurosci, 2009. **3**: p. 14.
690 68. Johnson, V.E., et al., *Inflammation and white matter degeneration persist for years after a*
691 *single traumatic brain injury.* Brain, 2013. **136**(Pt 1): p. 28-42.
692 69. Krstic, D., et al., *Systemic immune challenges trigger and drive Alzheimer-like*
693 *neuropathology in mice.* J Neuroinflammation, 2012. **9**: p. 151.

694 70. Schwarz, J.M., M.R. Hutchinson, and S.D. Bilbo, *Early-life experience decreases drug-induced*
695 *reinstatement of morphine CPP in adulthood via microglial-specific epigenetic programming*
696 *of anti-inflammatory IL-10 expression.* J Neurosci, 2011. **31**(49): p. 17835-47.
697 71. Brownell, K.D., et al., *The effects of repeated cycles of weight loss and regain in rats.* Physiol
698 Behav, 1986. **38**(4): p. 459-64.
699 72. Greenway, F.L., *Physiological adaptations to weight loss and factors favouring weight regain.*
700 Int J Obes (Lond), 2015. **39**(8): p. 1188-96.
701 73. Jia, M., et al., *Biomarkers in an animal model for revealing neural, hematologic, and*
702 *behavioral correlates of PTSD.* J Vis Exp, 2012(68).
703 74. Li, R., et al., *SOAP: short oligonucleotide alignment program.* Bioinformatics, 2008. **24**(5): p.
704 713-4.
705 75. Kim, D., B. Langmead, and S.L. Salzberg, *HISAT: a fast spliced aligner with low memory*
706 *requirements.* Nat Methods, 2015. **12**(4): p. 357-60.
707 76. Benelli, M., et al., *Discovering chimeric transcripts in paired-end RNA-seq data by using*
708 *EricScript.* Bioinformatics, 2012. **28**(24): p. 3232-9.
709 77. Shen, S., et al., *rMATS: robust and flexible detection of differential alternative splicing from*
710 *replicate RNA-Seq data.* Proc Natl Acad Sci U S A, 2014. **111**(51): p. E5593-601.
711 78. Langmead, B. and S.L. Salzberg, *Fast gapped-read alignment with Bowtie 2.* Nat Methods,
712 2012. **9**(4): p. 357-9.
713 79. Moskon, M., *CosinorPy: a python package for cosinor-based rhythmometry.* BMC
714 Bioinformatics, 2020. **21**(1): p. 485.
715 80. Hanzelmann, S., R. Castelo, and J. Guinney, *GSVA: gene set variation analysis for microarray*
716 *and RNA-seq data.* BMC Bioinformatics, 2013. **14**: p. 7.
717 81. Kumar, L. and E.F. M, *Mfuzz: a software package for soft clustering of microarray data.*
718 Bioinformation, 2007. **2**(1): p. 5-7.

719
720
721
722
723
724

Figure legends

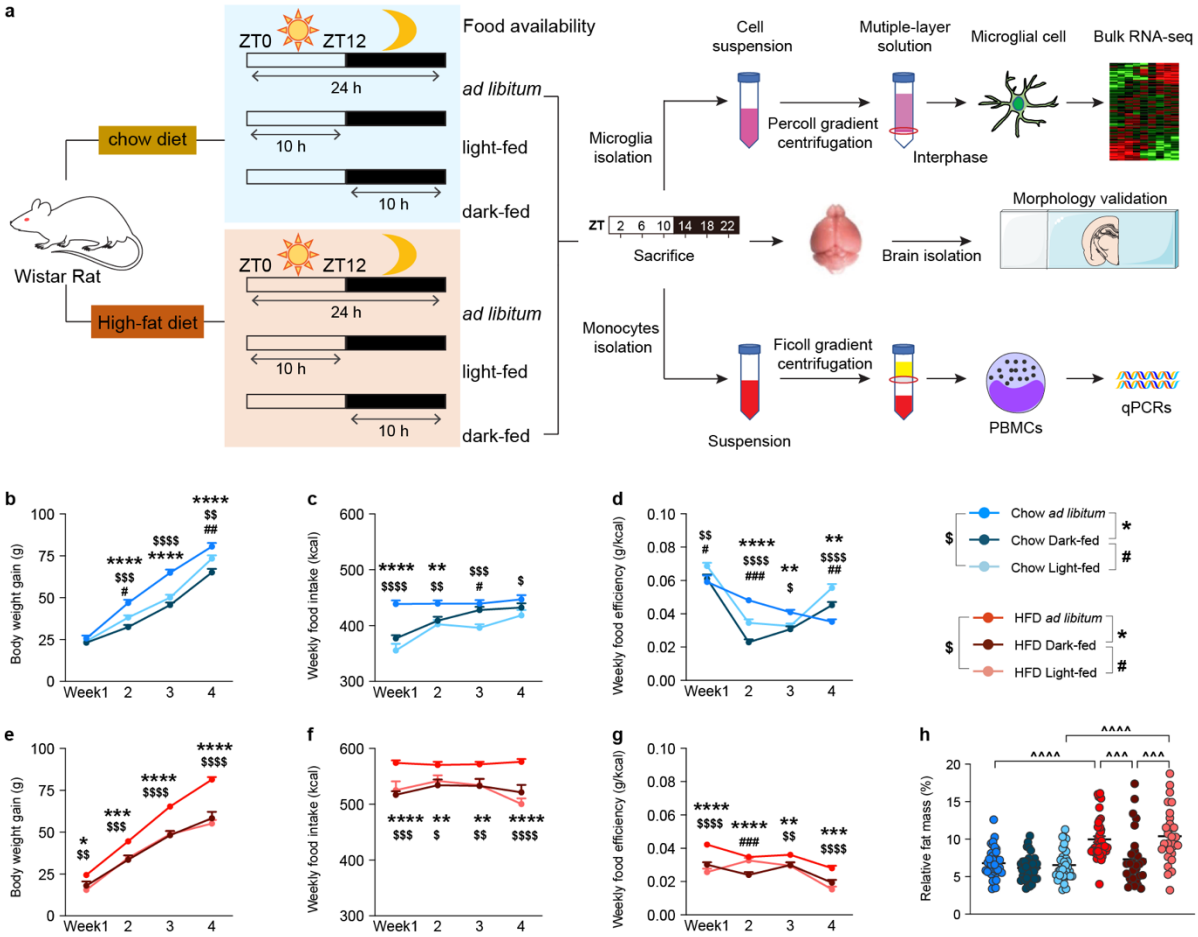

Fig.1 Time-restricted feeding with chow diet or high fat diet differentially affects metabolic parameters. **a,** Scheme illustrates the experimental design, showing different cohorts of Wistar rat with time-restricted access to chow diet or high fat diet (HFD) within a 24-hour day, and the strategy used for isolation of microglia or peripheral blood mononuclear cells (PBMCs) and morphological profiling. ZT0 = lights on, ZT12 = lights off; Light-fed: ZT1-ZT11 (10h), Dark-fed: ZT13-ZT23 (10h), *ad libitum*: free access to food (24h).

b-g, The dynamic changes in weekly body weight gain, food intake, and food efficiency under *ad libitum*, light-fed, and dark-fed conditions on chow diet (**b, d, f**) or high-fat diet (HFD) (**c, e, g**). **h**, Relative fat mass in all conditions just before sacrifice. Data are shown as mean ± SEM, data and were analysed by two-way ANOVA with repeated measures (*, #, $ $p< 0.05$, **, ##, $$ $p<0.01$, ***, ###, $$$, ^^^ $p<0.001$, ****, ####, $$$$, ^^^^ $p<0.001$).

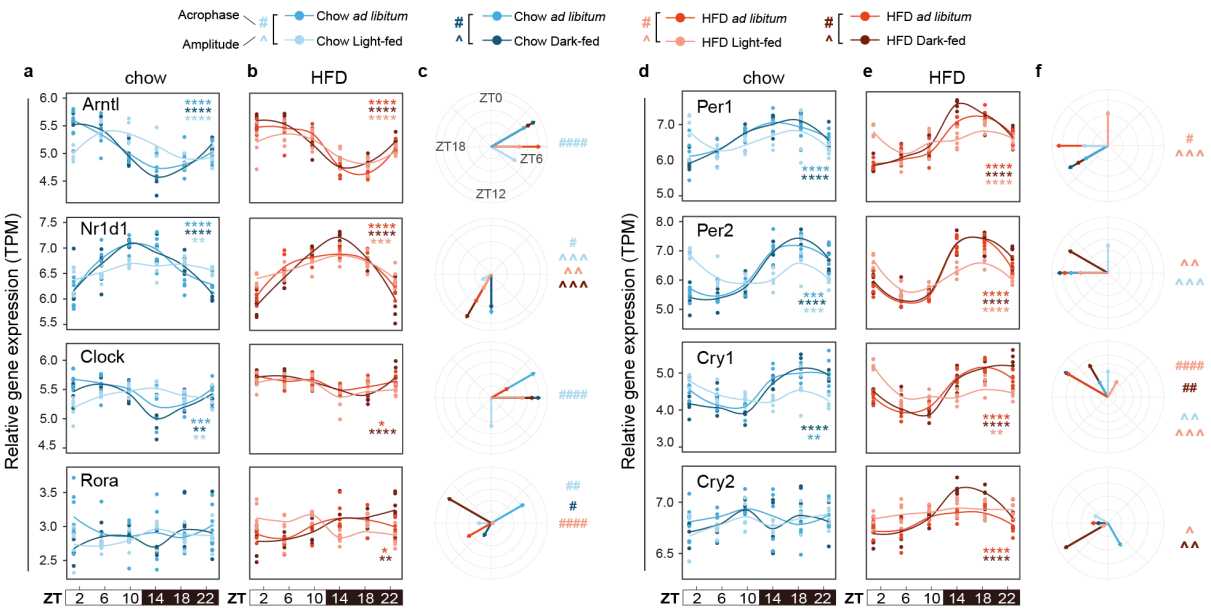

Fig.2 TRF during the light phase alters acrophase and/or amplitude of microglial core clock gene expression.

a,b,d,e, Relative gene expression of core clock genes in different feeding patterns under Chow **(a,d)** and HFD **(b,e)** conditions over time (timepoints from ZT2 to ZT22, at 4-hour intervals). Coloured asterisks in the upper or lower right corner indicate a significant 24-hour rhythm according to Consinor. $^{*}P < 0.05$, $^{**}P < 0.01$, $^{***}P < 0.001$, $^{****}P < 0.0001$. **c,f,** Spider plots show acrophase (coloured arrow) and amplitude (length of the coloured arrow) alterations of core clock genes. Coloured carets (^)and number signs (#) represent significant differences in amplitude and acrophase, respectively. $^{\#,\wedge}P < 0.05$, $^{\#\#,\wedge\wedge}P < 0.01$, $^{\#\#\#,\wedge\wedge\wedge}P < 0.001$, $^{\#\#\#\#,\wedge\wedge\wedge\wedge}P < 0.0001$.

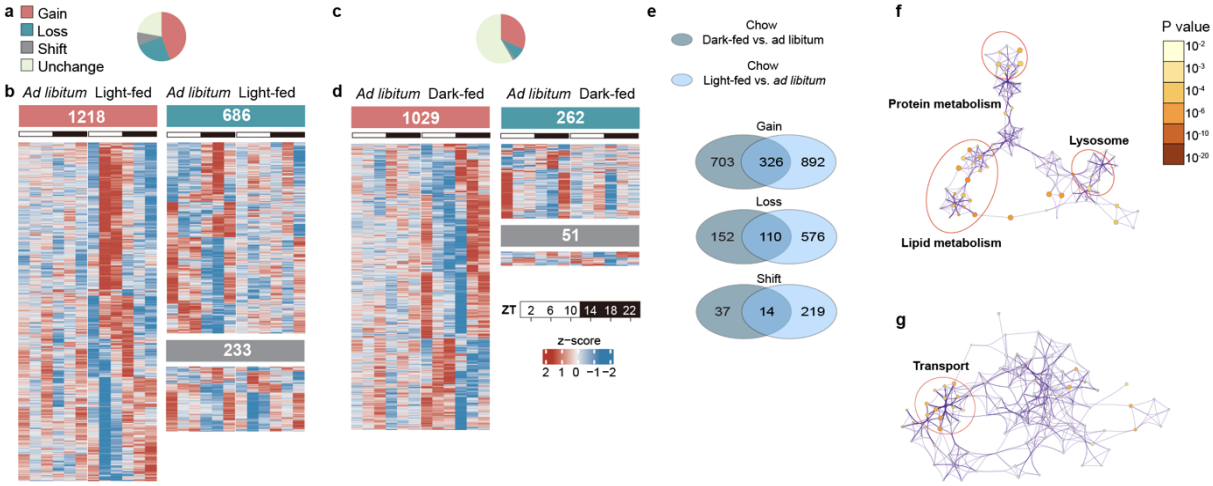

Fig.3 Time-restricted feeding in the light- or dark-phase with chow diet induces a significant gain of rhythmicity in gene expression, whereas feeding restricted to the light-phase also induces a robust loss of rhythmicity in gene expressions.

a-d, Pie charts depict the percentages of gained, lost, shifted, and unchanged genes relative to the total number of rhythmic genes in different comparisons in the chow groups (**a,c**). Heatmaps display the z-scored normalized transcript expression levels in different comparisons. Transcript expression profiles were categorized based on differential rhythmicity analysis using CompareRhythmR [42]. The three consecutive heatmaps, depict alterations in gained, lost, and shifted genes with the numbers in the unfilled rectangles representing the total gene counts for each category (**b,d**). **e,** Venn diagrams illustrate the identical counts of gained, lost, and shifted genes in chow comparisons. **f,g,** Pathway enrichment analysis of overlapping genes in the chow dark-fed vs. *ad libitum* and chow light-fed vs. *ad libitum* comparison using Metascape reveals networks of enriched terms in the genes that gained rhythmicity (**f**) and the genes that lost rhythmicity (**g**).

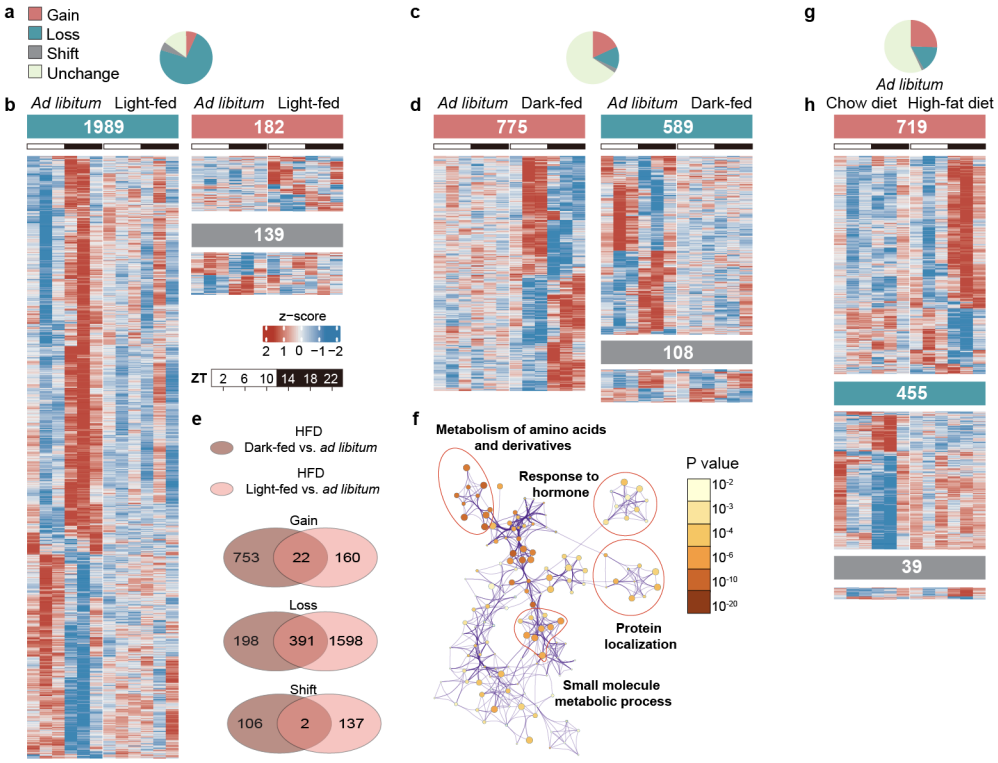

Fig.4 Time-restricted feeding in the light-phase combined with HFD induces the highest loss of rhythmicity in microglial gene expressions.

a-d, Pie charts depict the percentages of gained, lost, shifted, and unchanged genes relative to the total number of rhythmic genes in different comparisons in the HFD condition (**a,c**). Heatmaps display the z-scored normalized transcript expression levels in different comparisons. Transcript expression profiles were categorized based on differential rhythmicity analysis using CompareRhythmR [42]. The three consecutive heatmaps, depict alternations in gained, lost, and shifted genes with the numbers in the unfilled rectangles representing the total gene counts for each category (**b,d**). **e,** Venn diagrams illustrate the identical counts of gained, lost, and shifted genes in both chow and HFD comparisons. **f,** Pathway enrichment analysis of overlapping genes that lost rhythmicity in the HFD dark-fed vs. *ad libitum* and HFD light-fed vs. *ad libitum comparisons*. **g,** Pie chart depicting the percentages of gained, lost, shifted, and unchanged genes relative to the total number of rhythmic genes in chow *ad libitum* vs HFD *ad libitum*. **h,** Heatmaps displaying the z-scored normalized transcript expression levels in chow *ad libitum* vs HFD *ad libitum*.

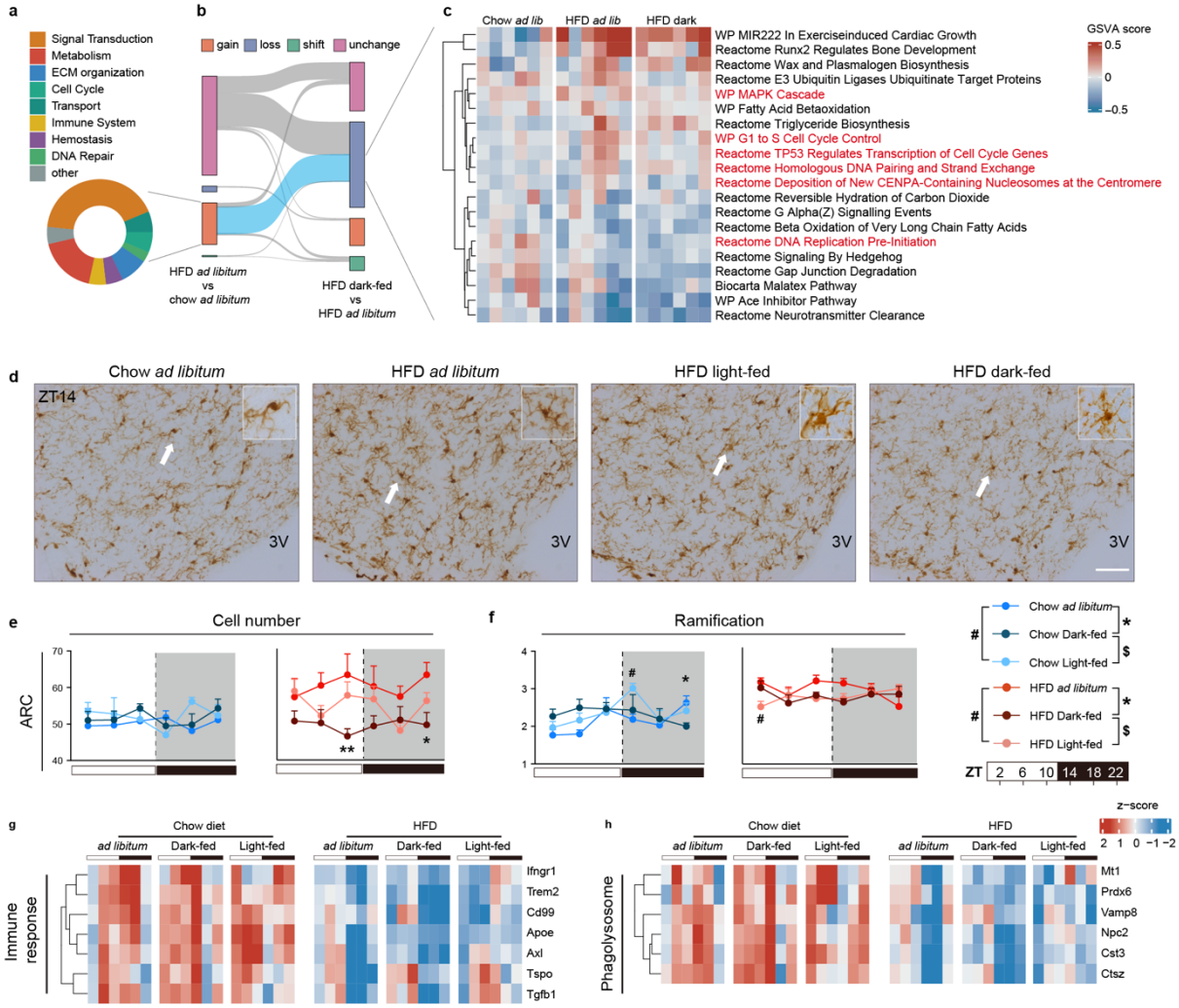

Fig.5 HFD restricted to the dark phase significantly reduces microglial cell number in the ARC.

a, Patheay categories involved in genes with gained rhythmicity in HFD *ad libitum* vs. chow *ad libitum* were mainly involved in signal transduction, metabolism and extracellular matrix (ECM) organization pathways. **b,** Sankey diagram illustrates alternations in gain, loss, shift, and unchanged categories between different comparison groups. **c,** Enriched pathways, based on the WikiPathways (WP), Reactome Pathway and Biocarta Pathways databases, depicted are pathways related to the transition from gained rhythmicity in HFD vs. chow *ad libitum* to lost rhythmicity in HFD dark-fed vs. *ad libitum*. Pathways highlighted in red are specifically associated with the cell cycle. Heatmaps display the z-scored normalized transcript expression levels. **d,** Representative figures of Iba1-ir microglia in the arcuate nucleus (ARC) at ZT14. The microglial cells in the high-magnification images in the upper right corner are indicated by a white arrow in the overview image. **e,f,** Quantifications of microglial cell number **(e)** and ramifications **(f)** in the ARC (0.16mm^2). Scale bars = 50 μm. 3V = the third ventricle. Iba1= Ionized calcium binding adaptor molecule 1. **g,h,** Heatmaps depict alterations in immune response (**g**) and phagolysosome (**h**). From left to right, the first three columns represent the ad libitum, light-fed, and dark-fed patterns under the chow diet condition, and the subsequent three columns correspond to the ad libitum, light-fed, and dark-fed patterns under the high-fat diet condition. Heatmaps display the z-scored normalized transcript expression levels. Data are shown as mean ± SEM, P values are analysed by two-way ANOVA with repeated measures ($^{*, \#, \$}$ $p < 0.05$, $^{**, \#\#, \$\$}p<0.01$, $^{***, \#\#\#, \$\$\$}p<0.001$).

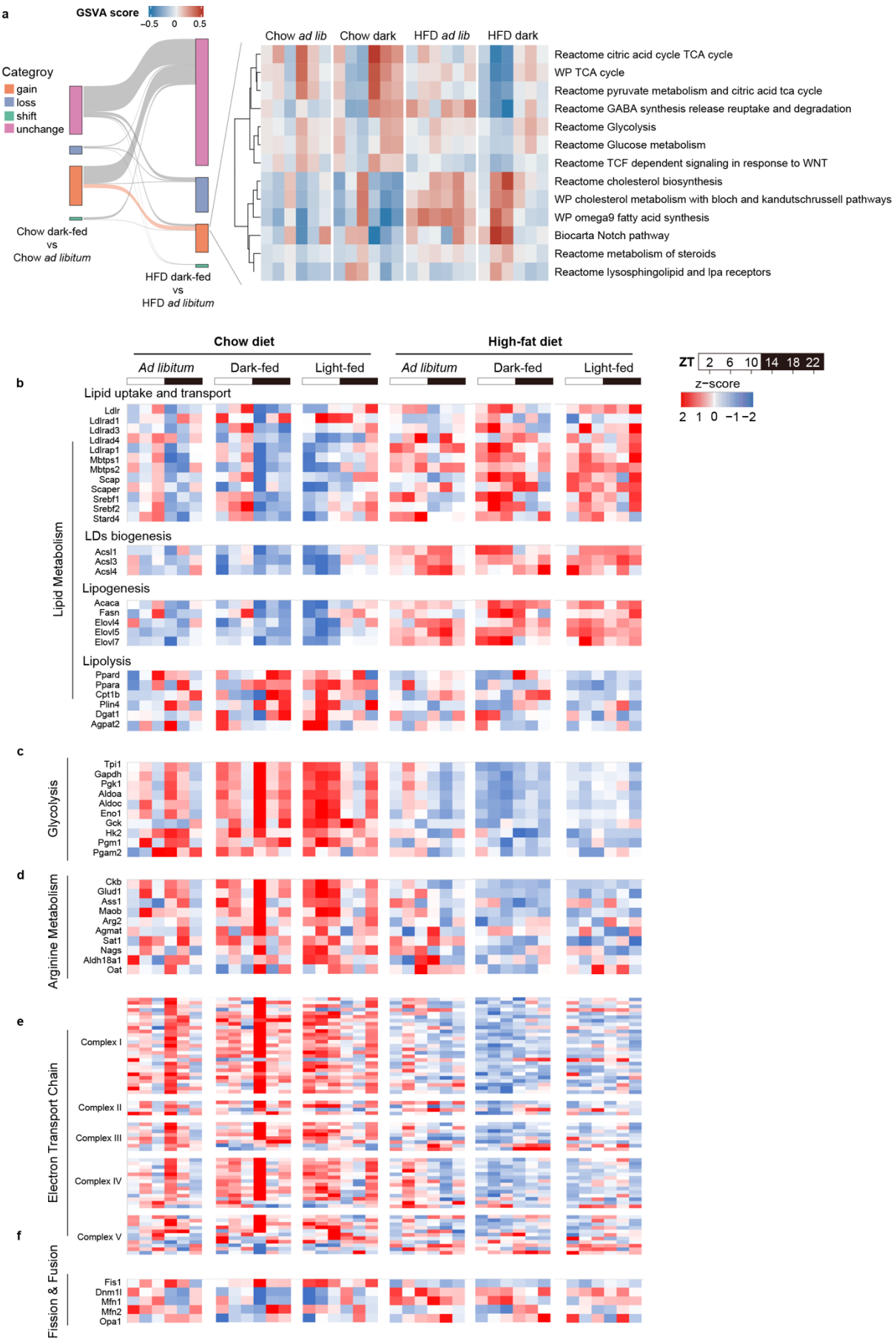

Fig.6 TRF is unable to reverse the detrimental effects of HFD.

818 **a,** Sanky diagram shows enriched pathways, based on the WikiPathways (WP), Reactome Pathway and Biocarta
819 Pathways databases, related to changes in rhythmicity in chow dark-fed vs. ad libitum and HFD dark-fed vs. ad
820 libitum conditions. **b-f,** Heatmaps depict alterations in lipid metabolism (**b**), glycolysis (**c**), arginine metabolism (**d**),
821 and electron transport chain (**e**), as well as mitochondrial fission and fusion processes (**f**). From left to right, the
822 first three columns represent the ad libitum, light-fed, and dark-fed patterns under the chow diet condition,
823 whereas the subsequent three columns correspond to the ad libitum, light-fed, and dark-fed patterns under the
824 high-fat diet condition.
825
826

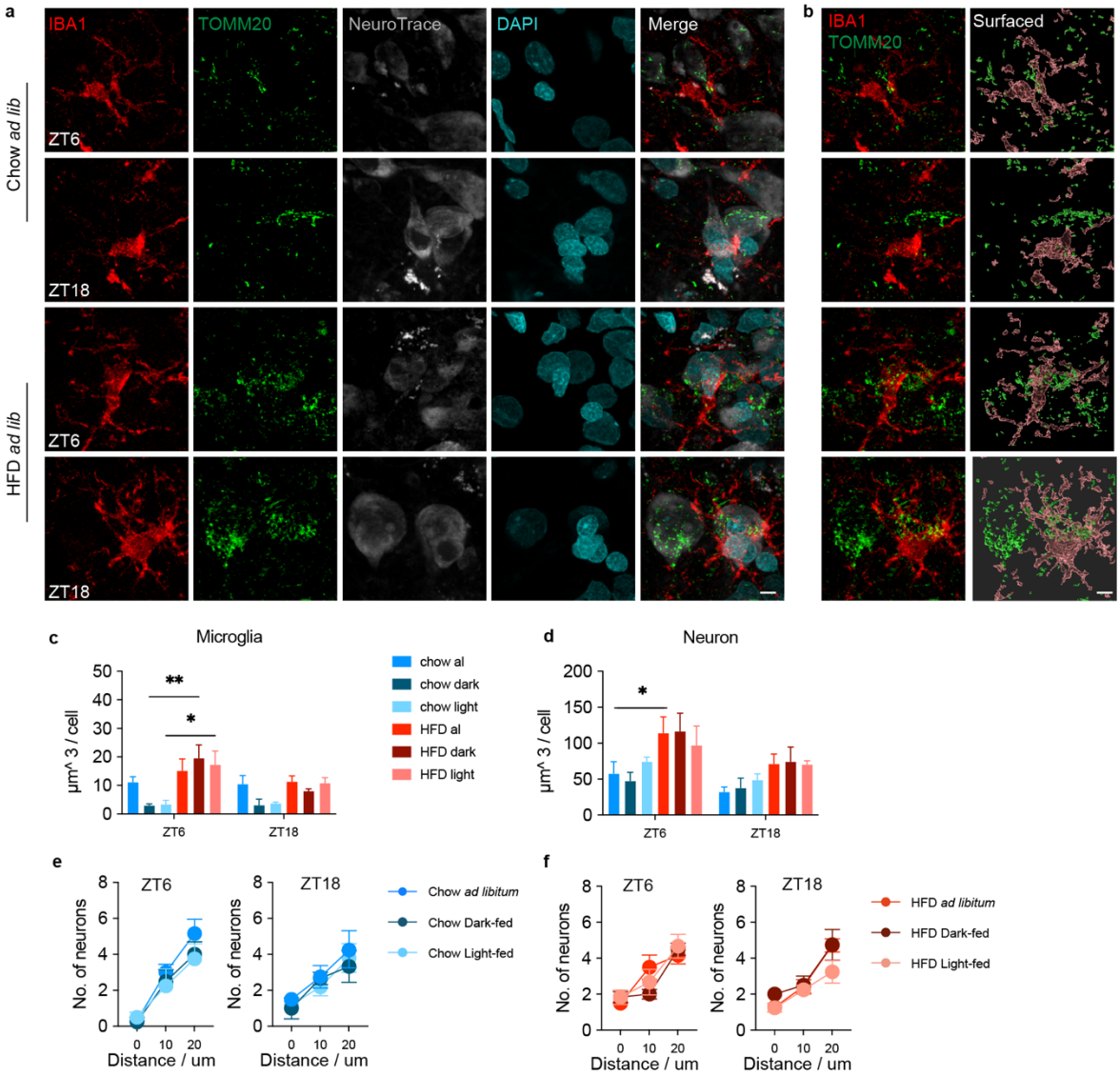

Figure 7. Mitochondrial alterations and neuron-microglia interactions in response to HFD and TRFs. **a,** Representative confocal images showing colocalization of Iba1 (red, microglial marker), Tomm20 (green, mitochondrial marker), NeuroTrace (gray, neuronal marker) and DAPI (nuclear marker) in the hypothalamus across different dietary conditions (Chow *ad libitum*, HFD *ad libitum*) at circadian time points ZT6 and ZT18. Scale bar: 5 μm. **b,** Surface rendering of microglial Tomm20 (green) and Iba1 (red) showing mitochondrial distribution in microglia. Scale bar: 5 μm. **c,d,** Quantification of microglial and neuronal Tomm20 volume in all groups at both ZT6 and ZT18. **e,f,** Quantification of the spatial distance between neurons and microglia in the Chow diet and HFD diet groups. Data are shown as mean ± SEM, P values are analysed by two-way ANOVA with repeated measures. Statistical significance is indicated as *p < 0.05, **p < 0.01.

Supplementary figure legends

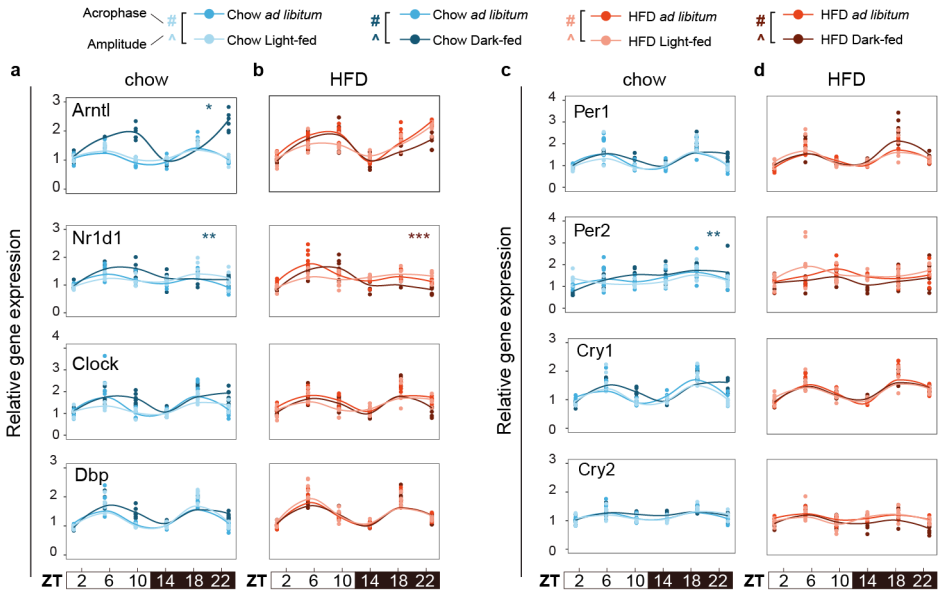

Extended Fig.1 TRF effects on molecular clock gene expression in PBMCs

a-d, Relative daily gene expression of 8 core clock genes during various feeding patterns under Chow **(a,c)** and HFD **(b,d)** conditions (timepoints from ZT2 to ZT22, at 4-hour intervals). Coloured asterisks in the upper right corner indicate adjusted p-values [adj P] obtained from JTK analysis for different feeding patterns: $^{*}P < 0.05$, $^{**}P < 0.01$, $^{***}P < 0.001$. Coloured carets (^) represent amplitude and number signs (#)acrophase significance. $^{\#,\ \wedge}P < 0.05$, $^{\#\#,\ \wedge\wedge}P < 0.01$, $^{\#\#\#,\ \wedge\wedge\wedge}P < 0.001$, $^{\#\#\#\#,\ \wedge\wedge\wedge\wedge}P < 0.0001$.

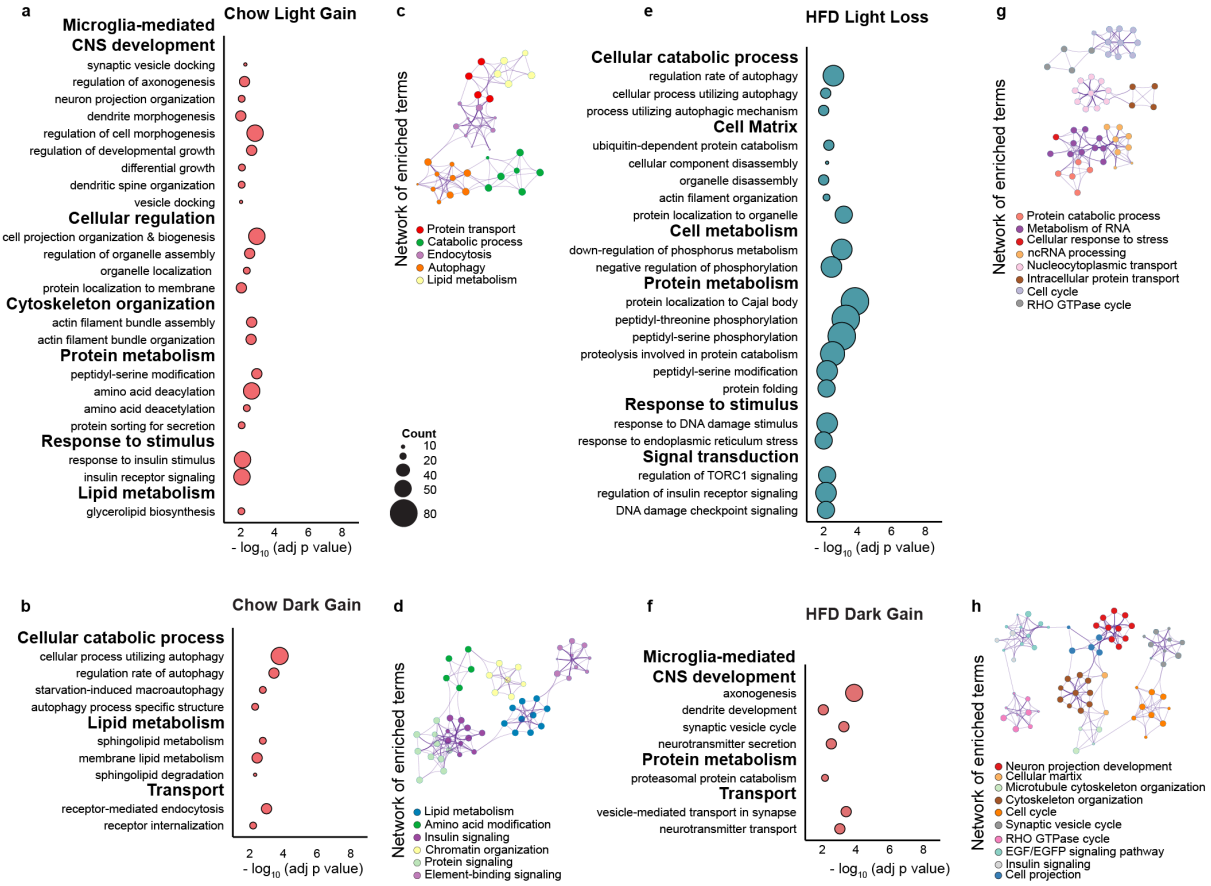

Extended Fig.2 Pathway enrichment analyses in gene groups associated with rhythmic alterations. **a,b,** Gene ontology terms for differentially expressed rhythmic genes. Dot size corresponds to the number of genes associated with each pathway, and -log10 adjusted p-value thresholds are shown on the x-axis. Enlarged and bold terms serve as summaries of sub pathways. Pink dots indicate pathways associated with gained rhythmicity genes in chow Light-fed vs. *ad libitum* (**a**) and chow Dark-fed vs. *ad libitum* (**b**). **c,d,** Network of enriched terms coloured by cluster ID, where nodes that share the same cluster have the same colour. Dots coloured by different pathway categories are indicated below. Network enrichment in genes that gained rhythmicity in chow Light-fed vs. *ad libitum* (**c**) and chow Dark-fed vs. *ad libitum* (**d**). **e,f,** Green dots represent pathways associated with genes that lost rhythmicity in HFD Light-fed vs. *ad libitum* (**e**). Pink dots indicate pathways associated with genes that gained rhythmicity in HFD Dark-fed vs. *ad libitum* (**f**). **g,h,** Network enrichment in genes that lost rhythmicity in HFD Light-fed vs. *ad libitum* (**g**) and genes that gained rhythmicity in HFD Dark-fed vs. *ad libitum* (**h**).

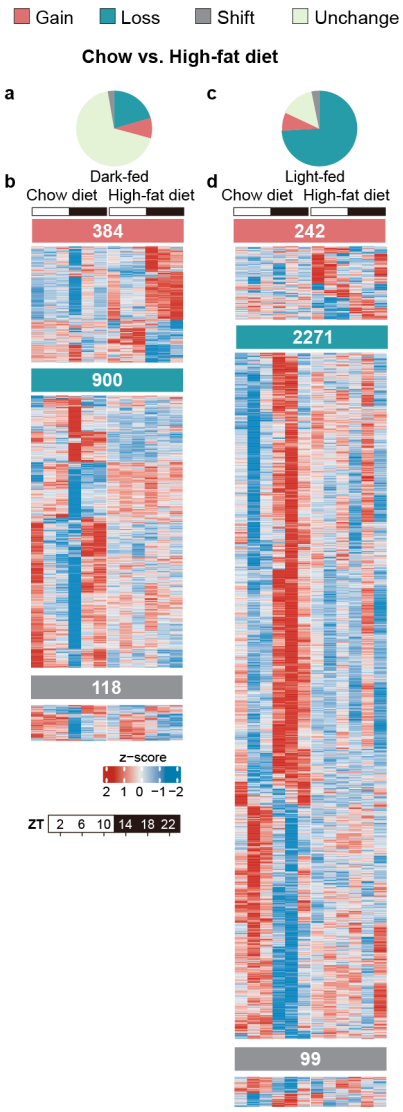

Extended Fig.3 Microglial gene expression alternations in HFD compared to chow for the dark-fed and light-fed groups.

a-d, Same arrangement strategy as shown in Fig.1, pie charts represent the proportions of genes that gained, lost, shifted rhythmicity or remained unchanged compared to the total number of rhythmic genes in different comparisons (**a,c**). In the bottom section, the heatmaps are categorized based on differential rhythmicity analysis using CompareRhythmR in dark-fed chow vs. HFD (**b**) and light-fed chow vs. HFD (**d**).

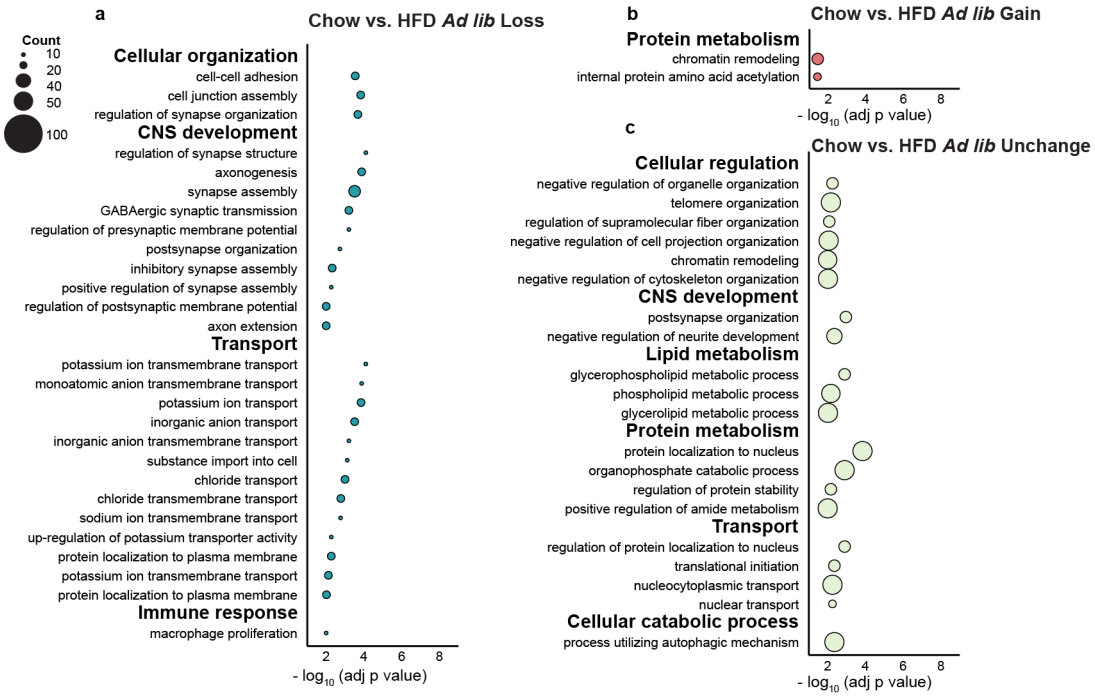

Extended Fig.4 Enriched pathways in loss, gain and unchanged categories based on gene ontology in chow vs. HFD *ad libitum*.

a-c, Pathways involved lost (**a**), gained (**b**) and unchanged genes (**c**) in the chow vs. HFD *ad libitum* comparison. Enlarged and bold terms serve as summaries of sub pathways. Dot size corresponds to the number of genes associated with each pathway, and $\log_{10}$ adjusted p-value thresholds are shown on the x-axis.

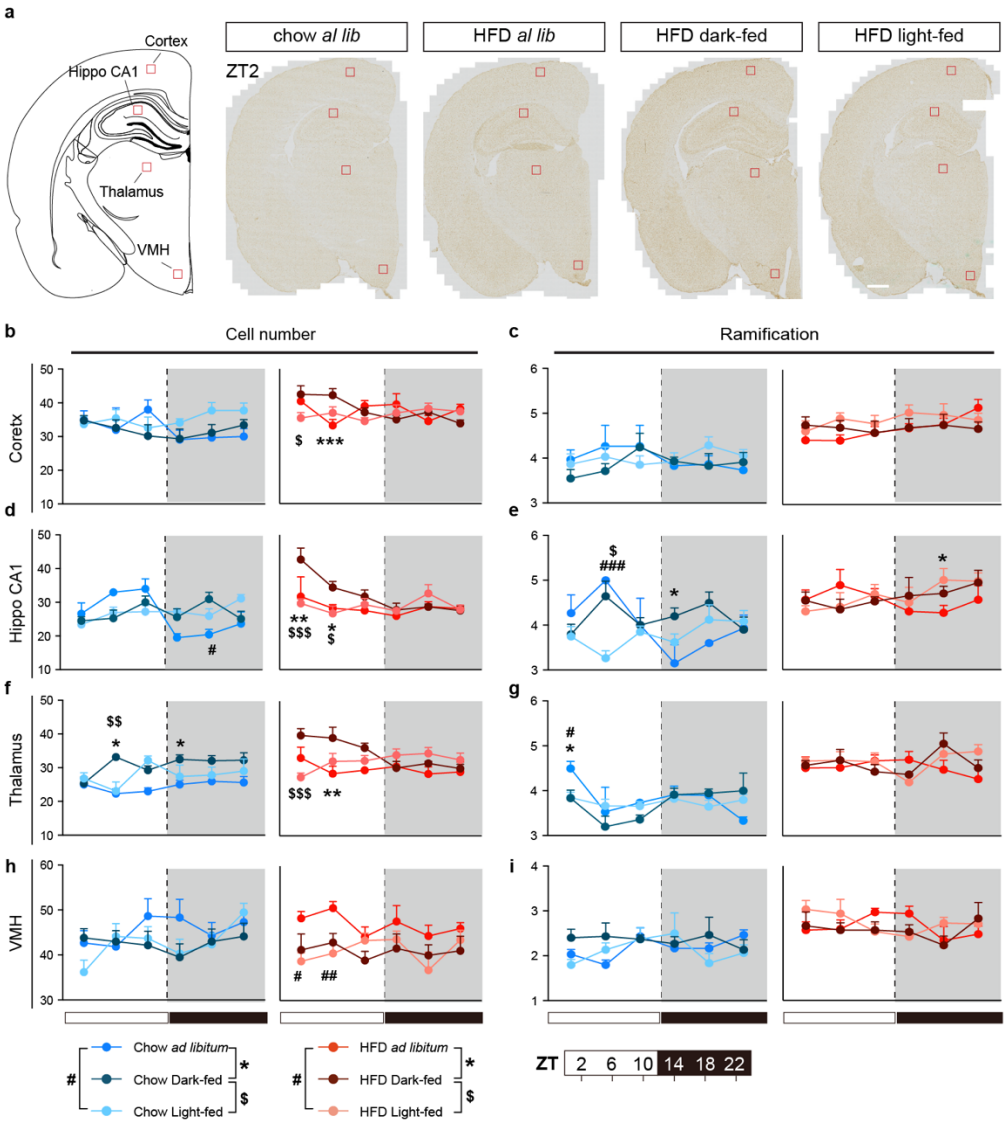

Extended Fig.5 Microglial morphological validation in different brain regions.

a, Brain regions are shown as small red rectangles in the transversal brain section in different groups. **b-i,** Quantifications of microglial cell number and ramifications in the cortex (**b,c**), hippocamus CA1 (**d,e**), thalamus (**f,g**) and the ventromedial nucleus of the hypothalamus (VMH) (**h,i**). Data are shown as mean ± SEM, and were analysed by two-way ANOVA with repeated measures (*, #, $ $p< 0.05$, **, ##, $$ $p<0.01$, ***, ###, $$$ $p<0.01$).

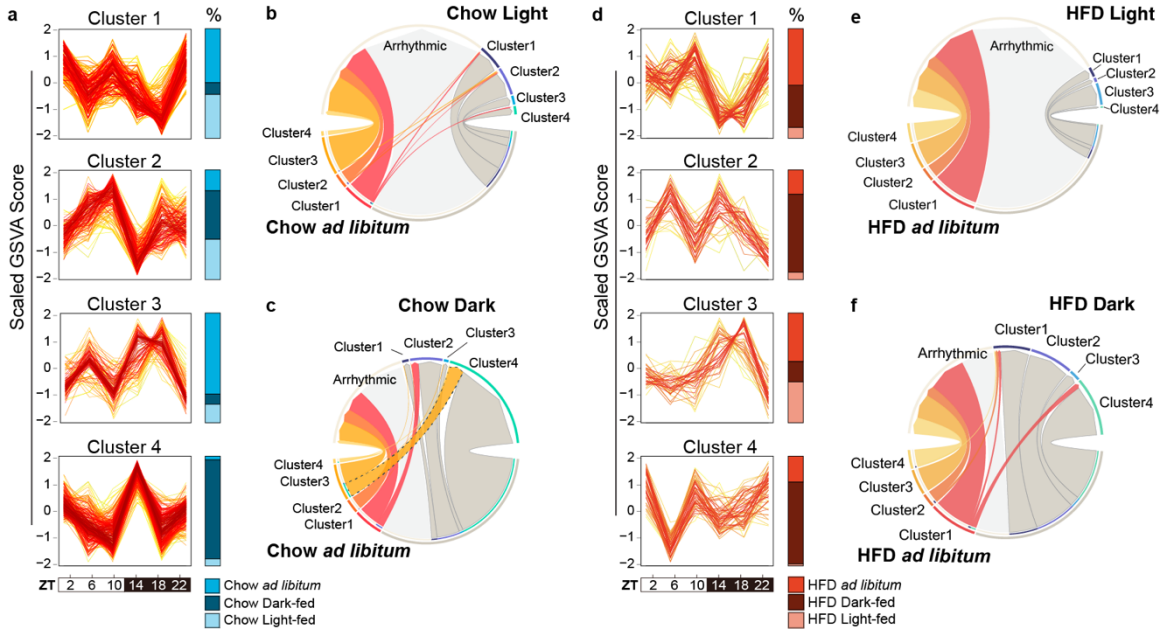

Extended Fig.6 HFD reduces the number of clustered pathways.

a, The Mfuzz algorithm was applied to cluster pathways resulting in four distinct clusters. The blueish column on the right represents the proportion in % of signalling pathways within different groups across clusters. **b,c,** Chord plot illustrates the alternations of the 4 clusters of pathways between chow light-fed vs. *ad libitum* (**b**), and chow dark-fed vs. *ad libitum* (**c**). The colours at the edge of the circles indicate different clusters. **d,** The Mfuzz algorithm illustrates four pathway clusters across all feeding patterns under the HFD condition. The reddish column on the right represents the proportion of signalling pathways within different groups across these clusters. **e,f,** Chord plot illustrates the alternations of the 4 clusters between HFD light-fed vs. *ad libitum* (**e**), and HFD dark-fed vs. *ad libitum* (**f**). The colours at the edge of the circles indicate different clusters.